Modeling Uncertainties for Passive Microwave Precipitation Retrieval: Evaluation of a Case Study

Alessandra Tassa, Sabatino Di Michele, Alberto Mugnai, Frank Silvio Marzano, *Senior Member, IEEE*, Peter Bauer, and José Pedro V. Poiares Baptista

***Abstract*—Physically based microwave spaceborne techniques for rainfall retrieval are usually trained by simulated cloud-radiation databases (CRDs) composed of cloud profiles and associated brightness temperatures (TBs). When generating the database, the evaluation of the associated modeling uncertainties is crucial for retrieval error estimation. However, this is extremely complex due to the large number of free parameters. In this work, a possible methodology for taking into account CRD-related modeling uncertainties is proposed. The methodology—fairly general—is here applied to a limited dataset (a cloud-model resolved numerical output of a tropical cyclone). The modeling errors are obtained from systematic TB sensitivity tests associated to several parameters: particle sizes, temperature, ice content, sea surface wind speed, viewing angle, footprint size, radiative transfer schemes, melting phase, and particle shape. TB uncertainties are eventually summarized in a modeling error covariance matrix representing the intrinsic variability of the generated CRD. For comparison with real observations, the TBs are simulated at the spatial resolution, viewing geometry and frequencies of the Tropical Rainfall Measuring Mission (TRMM) Microwave Imager (TMI). The matrix is evaluated with respect to TMI data in terms of an indicator called database matching index. Since they are based on a single case study and suffer from the lack of direct coupling of the radiative transfer with the cloud-resolving model, the provided results should not be considered an exhaustive evaluation of cloud-radiation modeling errors. Nevertheless, they may be considered a valuable starting point for error characterization, since extensions to larger databases could definitely improve modeling error budgets.**

***Index Terms*—Error modeling, estimation uncertainties, retrieval.**

I. Introduction

MICROWAVE imagers have proven to be a valuable tool for inferring precipitation from space. Especially in the last two decades, a large number of satellite missions allow to study precipitation and clouds—among these, the Special Sensor Microwave/Imager (SSM/I), the Tropical Rainfall Measuring Mission (TRMM) Microwave Imager (TMI) [1] and the Advanced Microwave Scanning Radiometer (AMSR).[1] The Global Precipitation Mission (GPM), composed of a constellation of several TMI-like and SSM/I-like passive microwave radiometers,[2] is envisioned for the future.

Inversion techniques for rainfall retrievals from passive microwave measurements infer the physical characteristics of the observation targets from their radiative signatures. A large number of retrieval algorithms have been proposed and applied—see [2] and [3] for comprehensive descriptions of several SSM/I algorithms, as well as [4]–[7] for retrieval algorithms employing TRMM data. In general, all these algorithms are trained by *a priori* information taken from simulated cloud-radiation databases (CRDs) consisting of statistically significant sets of precipitation profiles and associated radiances or brightness temperatures (TBs). The training CRDs may be derived from empirical analyses as well as from numerical cloud-resolving model simulations. In the latter case, these methods are generally referred to as "physically based," and they are exhaustively described in the literature (e.g., [8]–[11]). One of the main shortcomings of all algorithms is that their performance entirely depends on the representativeness and correctness of the database. Thus, it is extremely important to estimate the uncertainties and error sources that are part of the generation of the CRD. This error analysis is also fundamental for data assimilation techniques based on variational methods.

Physically based inversion techniques, trained by *a priori* model-derived information, must take into account both model and measurement error characteristics. In particular, Bayesian retrieval schemes—under the assumption of Gaussian error distribution $p(\mathbf{y}_0 - \mathbf{y}(\mathbf{x}))$—explicitly require the evaluation of the model $(\mathbf{M})$ and measurement $(\mathbf{O})$ error covariance matrices, defined by the following multidimensional probability density function:

$$p\left(y_0 - y(x)\right) \sim \exp\left\{-\frac{1}{2}\left(y_0 - y(x)\right)^T \left(\mathbf{M} + \mathbf{O}\right)^{-1} \left(y_0 - y(x)\right)\right\} \quad (1)$$

where $\mathbf{y}_0$ represents the observation vector and $\mathbf{y}(\mathbf{x})$ the modeled radiance vector (e.g., see [12] and [13]). In (1), $\mathbf{O}$ accounts for the observation errors (i.e., instrumental noise), while $\mathbf{M}$ encompasses all uncertainties related to the forward modeling[3] (i.e., in the generation of the *a priori* information database). $\mathbf{M}$ and $\mathbf{O}$ are usually assumed to be uncorrelated (see

Manuscript received August 13, 2004; revised August 12, 2005. This work was supported in part by the Italian Space Agency (ASI) and in part by the European Space Agency.

A. Tassa and A. Mugnai are with the Istituto di Scienze dell'Atmosfera e del Clima (ISAC), Consiglio Nazionale delle Ricerche (CNR), 00133 Roma, Italy (e-mail: a.tassa@isac.cnr.it).

S. Di Michele and P. Bauer are with the European Centre for Medium-range Weather Forecasts (ECMWF), Reading, RG2 9AX U.K.

F. S. Marzano is with the Department of Electronic Engineering, University "La Sapienza" of Rome, 00184 Rome, Italy and also with the Centro di Eccellenza CETEMPS, Università dell'Aquila, 67040 L'Aquila, Italy (e-mail: marzano@die.uniroma1.it).

J. P. V. Poiares Baptista is with the ESTEC-European Space Agency, 2200 AG Noordwijk, The Netherlands.

Digital Object Identifier 10.1109/TGRS.2005.860484

[1]http://www.aqua.nasa.gov/AMSRE3.htm

[2]http://gpm.gfsc.nasa.gov

[3]In our example, $\mathbf{M}$ comprises all approximations related to modeling precipitation/atmospheric fields and radiances.

[13]–[16]) and diagonal. In contrast to $\mathbf{O}$, the evaluation and quantification of $\mathbf{M}$ for cloud-radiation databases aimed at precipitation retrieval is fairly complicated due to unknown errors introduced during cloud and radiative transfer modeling. In order to compute $\mathbf{M}$ in a general way, all errors intrinsic to the generation of the model-derived parameters (from the mesoscale cloud-resolving model, to the radiative transfer (RT) model and the spaceborne sensor configuration model) should be taken into account. The ideal procedure for computing such errors could be sketched as follows.

1) Obtain the errors of the meteorological analysis the mesoscale cloud model was initialized with.
2) Obtain realistic error probability distributions of mesoscale cloud model parameterizations.
3) Run ensembles of combined mesoscale-RT model and evaluate the dispersion of modeling results in TBs-space.

Note that a similar technique was applied by [17] to define TB-signal variability from combined temperature/moisture and surface emissivity effects involving large-scale condensation, convection, and radiative transfer modeling. This procedure is extremely complex and would require rather costly ensemble modeling. Therefore, a limited approach has been followed here which is focused on the evaluation of RT model input errors, under the hypothesis that (small) perturbations of bulk cloud and environmental parameters can lead to an approximation of total modeling errors. The strong nonlinearity of the RT operator tends to filter the error probability distribution resulting in different error distributions for the computed radiances.

It is important to notice that in addition to modeling errors, inversion schemes have to tackle also the so-called "randomization problem" (i.e., the necessity of taking into account all variability associated to the same cloud structure, in order to get a sufficiently thorough and robust set of cloud structures). The problem has been handled in different ways (e.g., computing the TBs for a given three-dimensional (3-D) cloud structure under different background conditions—as in [4] and [7]—or through additional error injections—as in [5]). This variability is here considered as an additional modeling uncertainty.

In this work, a possible procedure for evaluating the modeling uncertainties associated to the generation of CRDs is introduced. The uncertainties are computed through sensitivity analyses aimed at evaluating the impact of various bulk cloud/radiative parameters on the resulting simulated radiance distributions. The parameters considered are: drop size distribution parameterization, temperature profile, ice water content, sea surface wind speed, viewing angle, antenna beamwidth, radiative transfer approximation, presence of melting phase, and particle shapes. The results of the sensitivity studies are summarized in a cloud-radiation database modeling error covariance matrix $\mathbf{M}_{\mathrm{CRD}}$. The matrix represents a measure of the confidence in the modeling assumptions. In fact, more than errors, we are here considering modeling uncertainties. When the CRD is used within retrieval schemes, these uncertainties would eventually translate into estimation uncertainties (see [13]). The TB "error" statistics can be thought in the inverse problem as "noise regulators." The extended CRD (i.e., the standard CRD completed with its own covariance matrix) is considered more representative and robust than the standard one and should ideally allow the retrieval of a wider range of cloud scenarios.

The results obtained in this study are a basic element of physically based Bayesian retrieval algorithms such as the Bayesian algorithm for microwave-based precipitation retrieval (BAMPR); see [16] and [18]. Note that complete indications on how to insert the database and its error covariance matrix in the inversion algorithms are given in [13].

The paper is organized as follows. In Section II, details about the generation and perturbation of the cloud-radiation database are given, and the impact of the various parameters on the simulated TBs is discussed. In Section III, results of the sensitivity study are summarized in the error covariance matrix definition. Finally, in Section IV the impact of the error covariance matrix on the matching between the manifolds of the simulated TBs and of the measurements for selected TMI case studies is analyzed. The agreement is evaluated by means of an extended database matching index (DMI); see [16].

II. Cloud-Radiation Database

A. Cloud-Radiation Database Generation

CRDs for physically based rainfall retrievals are usually composed of several sets of simulated sensor-dependent brightness temperatures[4] and hydrometeor profiles. They are generated by coupling radiative transfer schemes and cloud-resolving model simulations. In this study, for generating the CRD that is used by the BAMPR algorithm, one time step (minute 2130) of a mesoscale cloud model simulation of a tropical cyclone (Hurricane Bonnie; see [19]) performed with the University of Wisconsin Non-hydrostatic Modeling System (UW-NMS) [20] has been chosen. Even though such a limited database cannot be considered representative of different weather events, it satisfies our purpose of a detailed TB sensitivity study.

The microwave signature of the cloud model simulation has been computed as in [16]: the RT code is a 3-D-adjusted plane-parallel (also called "slanted-path plane-parallel"; see [21]) at TMI frequencies and viewing angle. Hydrometeor properties have been computed according to the Mie theory. Their sizes have been distributed according to constant-slope inverse-exponential size spectra, except for cloud droplets and ice crystals that are monodispersed (see also [22]). No melting phase has been considered for the control case. Sea surface emissivity has been computed according to [23], with a reference sea surface wind speed[5] of 15 m/s. Finally, since TBs are at cloud model resolution (here 2.5 km), the TMI antenna gain function is simulated for each channel.

B. Sensitivity Analysis of Cloud-Radiation Database

From the above, it is evident that the simulated brightness temperatures depend on a large variety of microphysical, environmental, and imaging modeling parameters, that can only be considered known with limited accuracy. In our study, the TB sensitivities to the following bulk parameters have been analyzed:

- particle size distribution;
- temperature profile;

[4]i.e., at the observing geometry, wavelength, resolution of the sensor.

[5]The wind speed at sea surface is not given by the cloud model.

TABLE I
PARAMETERS USED IN THE SENSITIVITY TESTS. REFERENCE VALUES/MODELS AND PERTURBATION RANGES ARE INDICATED FOR EVERY PARAMETER

PARAMETER	STANDARD MODEL / VALUE	MAXIMUM DEPARTURE ALLOWED	
		Absolute Range	*Percent*
Particle size distribution CS-MP *References : [22]*	λ_{RAIN} = 1.852 mm^{-1}	1.389 - 2.315 mm^{-1}	25%
	$\lambda_{GRAUPEL}$ = 2. mm^{-1}	1-3 mm^{-1}	50%
Sea surface wind speed *Reference: [23]*	15 m/s	7.5 - 22.5 m/s	50%
Temperature profile	Model (average SST: 300K)	± 3 C°	1%
Antenna beam width *Reference: [16]*	TMI IFOV		10%
Antenna pointing	53 ° (TMI viewing angle)	± 0.5°	1 %
High-density ice water content	Model	N/A	30%
Radiative transfer model	Slanted-path Plane Parallel *References: [21]; [36]*	Fully 3D Montecarlo model *Reference : [21]*	
Melting phase	No melting	*References: [43]; [40] and [41]*	
Particle shapes	Spherical	Randomized Oblate vs. sphere perturbation factor *Reference: [48]*	

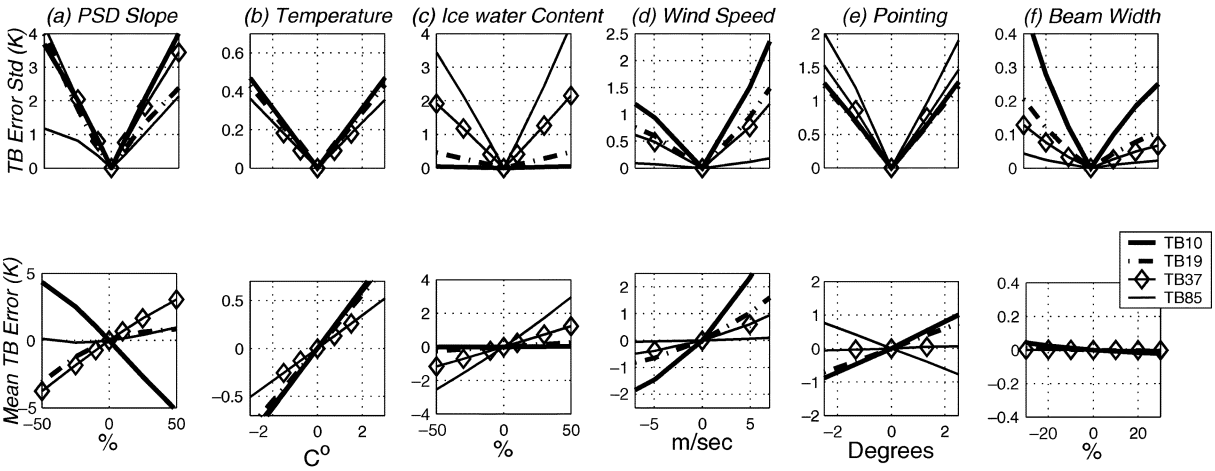

Fig. 1. Model TB uncertainties (standard deviations and mean) as function of the perturbation from the reference values for six different parameters and at four TMI frequencies. The parameters are as follows: (a) particle size distribution slope for constant-slope inverse-exponential, (b) profile temperature, (c) high-density ice water content, (d) sea surface wind speed, (e) antenna pointing angle, and (f) antenna beamwidth.

- high-density ice water content;
- sea surface wind speed;
- pointing instabilities;
- antenna beamwidth.

Every parameter has been examined independently, i.e., the standard procedure for computing the TMI-like brightness temperatures has been altered for one parameter at a time (e.g., changing only the PSD, only the viewing angle, and so on). Table I summarizes all the parameters that have been considered in our analysis and the tests that have been performed. For every test, the model parameter under examination has been randomly varied[6] within a given range (as indicated in the right column of Table I) about its reference value for every single vertical cloud structure (or surface pixel) of the considered dataset. Afterward, TBs have been computed over the whole perturbed 3-D structure and spatially filtered for simulating the TMI antenna pattern. Finally, the perturbed TBs have been compared with the ones from the control simulation (i.e., the ones computed by using the standard parameters) for evaluating the deviations that can be expected when using the altered parameters. Note that because of the 3-D approach every point of the final database encompasses a great variety of possible variations of pixels and profiles and may be regarded as an overall effect of the free parameter variation over a wide range of possible cloud structures.

Fig. 1 shows the effect of the perturbations for the selected parameters in terms of means and standard deviations of the TB departures with respect to the reference values at four TMI frequencies. The TB deviations (upper row) indicate the sensitivity

[6]The simplistic uniform error distribution has been adopted in order to follow a conservative approach due to lack of more detailed reliable information. Different variation spectra could be adopted, but it is believed that realistic spectra could be derived only from direct coupling with a cloud model.

of the TBs to the various parameters and describe the dispersion of the TB-manifold. These are always increasing functions of the amount of the parameter perturbations but the curves are not symmetric with regard to zero and strongly depend on frequency. Biases (lower row) are in many cases not negligible.

The panels are separately commented for each parameter in the following text.

Particle Size Distribution: The size spectra of the hydrometeors have a very large impact on the radiative properties of clouds and precipitation. As pointed out by [22] and [24], particle size distributions (PSDs) are one of the main sources of uncertainty in simulated brightness temperatures at microwave frequencies. A large number of PSD parameterizations exists. For rain PSDs, several models have been proposed—e.g., [25]–[28], among many others. PSDs of precipitating ice are even more uncertain [29], [30], and their ambiguities are expected to have an extremely important effect on brightness temperatures at high microwave frequencies (see [31]).

In our tests, we have used the PSDs specified by the cloud model itself: i.e., constant-slope inverse exponential. Cloud droplets and ice crystals have been assumed monodispersed. The effect of PSD modeling on the upwelling TBs has been analyzed in detail by randomly varying the value of the slope for constant-slope inverse-exponential PSDs. Perturbations as large as 50% correspond to variations of the characteristic diameter from 0.027 to 0.081 cm for rain drops and from 0.025 to 0.075 cm for graupel particles. These changes have a very large impact on the radiative properties of the cloud and therefore on the TBs. Fig. 1(a) shows the effect of perturbing the PSD slopes for both rain drops and graupel particles. The highest sensitivity is shown at 37 GHz. Surprisingly, also 19 GHz and even 10 GHz show large sensitivity to these perturbations. At 10 GHz, the emitted radiation is mainly related to precipitating liquid water. At 19 GHz, the TB is mostly related to the radiation emitted from the upper rainy layers but is also affected by the PSD of graupel particles. At 85 GHz, the contribution of graupel particles (and of their size spectra) is predominant. TB standard deviations can reach 4 K at 19 and at 37 GHz. The mean deviations are as large as -3 K (at 10 GHz). The most remarkable feature is that, while the 19- and 37-GHz curves show similar trends (from negative to positive values, increasing with the parameter perturbation), the 10-GHz curve shows an opposite trend. This is somewhat unexpected (the presence of large particles induces a TB-increase due to increased absorption), but could be related to the fact that in case of large water contents most radiation comes from the upper, cooler layers. Because of the large uncertainties associated with PSD modeling, we have allowed slope variations as large as 50% for graupel particles and 25% for rain drops, as shown in Table I.

Temperature Profile: Assessing the influence of the temperature profile on the radiative signatures of a given cloud scene is of extreme importance because it is equivalent to a change in climatic zone. Important TB-modifications are expected when the complete meteorological profiles are changed: for instance, [22] found warming as large as 40 K when imposing an observed meteorological profile (for both temperature and water vapor) of a tropical typhoon on a midlatitude supercell storm simulation. This was mainly due to increased emission at lower microwave frequencies. Obviously, the temperature profile is linked to pressure and water vapor profiles, as well as to the cloud profile itself. From a purely radiative point of view, temperature impacts on the emission properties of the atmosphere through the Planck function (changing the temperature of the emitted radiation) as well as on the radiative properties of the hydrometeors (especially for the liquid drops).[7] Finally, emission from sea surface is driven by temperature (through the emission physical temperature and sea surface emissivity),[8] but this effect may be neglected for rainy areas and high frequencies.

In our test we have randomly varied the temperature profile for each single vertical column before computing the RT calculations. No adjustment has been made on water vapor/pressure profiles or on the freezing level/hydrometeor distribution, so that we do not allow any temperature departure larger than ± 3 °C. From this, we have obtained small TB local deviations (less than 3 K), monotonically increasing/decreasing with temperature variation [see Fig. 1(b)]. The large sensitivity, shown at 10 GHz, depends on the effect of surface emissivity and on the fact that this frequency is mainly linked to emission. Biases are very small (0.6 K) and increase monotonically with the parameter variation at all frequencies.

High-Density Ice Water Content: One of the main difficulties in precipitation profile estimation is the evaluation of the amount of frozen water [33]. Mesoscale cloud models frequently predict excessive amounts of large ice particles above the freezing level, having no correspondence with radar and *in situ* measurements. In [7], [22], and [34], among others, it is claimed that the simulated radiative signatures of frozen top layers of cloud systems are not realistic and that in some cases there might be an overproduction of ice amounts about the freezing level produced by cloud models. In [4], a systematic discrepancy between TMI-only and PR-only profile estimates right above the freezing level was observed, the TMI-retrieval frequently overestimating the amount of ice.[9] The main difficulties seem to come from the uncertainties in ice particle modeling.

Tests have been performed so that the high-density graupel particles were converted to low-density snowflakes with varying proportion (up to a maximum of 30%). A similar conversion has been already proposed by [34] in order to get more realistic TB polarization differences. Since snowflakes—in contrast to graupel—are hardly visible at frequencies below 90 GHz, this experiment mainly affects the TBs at high frequencies. The results [see Fig. 1(c)] show an important effect (both in terms of standard deviations and of biases) at 37 GHz and, more markedly, at 85 GHz[10] (values as large as 20 K) and almost no effect at the lower frequencies.

[7]The imaginary part of the index of refraction of water decreases with temperature at 10 and 19 GHz, while it increases at 85 GHz. On the contrary, n_{ICE} can be considered approximately temperature-independent at all frequencies. See for example [32].

[8]The sea surface emissivity (SSE) is generally decreasing with temperature except at 10 GHz, where it has a slight increase for temperatures warmer than 20 °C (see [23]).

[9]The official TMI-only algorithm from the National Aeronautics and Space Administration is a physically based algorithm, very similar to BAMPR. Retrieved ice contents are driven from cloud-model simulations.

[10]The 85 GHz is in fact an optimal indicator of convection and is efficiently used for retrieving graupel amounts.

Sea Surface Wind Speed: Sea surface wind speed is a driving factor in determining sea surface emissivity through surface roughness. [23] model sea surface emissivity as a function of temperature, salinity, polarization, surface wind speed, viewing angle, and surface rainfall rates. From our tests, wind speed and observation angle account for most of the computed TB variations. Sea surface emissivity may be a crucial factor in biasing rainfall estimates, because it drives the surface (as well as the downward reflected) contribution to the TBs. Even though clouds and precipitation tend to attenuate the impact of surface characteristics on TBs, this effect can be significant at lower frequencies and in case of semitransparent clouds. As a matter of fact, we have computed TB differences at 10 GHz that may be as large as about 20 and 10 K for horizontal and vertical polarization, respectively, at model resolution. Moreover, pixels near the cloud edges usually contain cloud-free areas, thus enhancing the impact of surface emissivity. For inversion purposes, it is important to assess how the (unknown) background contributes to the upwelling radiation. Model "randomization" is particularly recommended since wind velocity may change very rapidly in space and time.

In our tests the wind speed for every cloud-model surface grid box is randomly varied between 7.5 and 22.5 m/s. The effect of the sea surface dominates the lower frequencies, while the high-frequency channels tend to rapidly saturate with increasing rain rate.[11] As shown in Fig. 1(d), the TB standard deviation increases with parameter perturbation. However, this behavior is not symmetric due to the nonlinear dependence of the sea-surface emissivity on the wind speed (see [23]), which shows an increasing growth rate for wind speeds larger than about 10 m/s at all frequencies. Biases increase with parameter perturbation. Fig. 1 shows that the effect of the surface decreases with wavelength. While it is relevant at 10 GHz for perturbation factors larger than 20% (i.e., ± 3 m/s), it is definitely negligible at 85 GHz because of the higher optical thickness.

Pointing Instabilities: Even in the case of conically scanning radiometers (ensuring a constant zenith angle of observation) the sensor viewing angle may undergo small fluctuations due to (small) instabilities of the platform and due to the nonsphericity of the Earth. This latter effect is generally negligible, but it becomes relevant for such a low-orbit satellite as TRMM. In fact, TMI viewing angles oscillate between 48° and 54°. Changing the viewing angle has a radiative (since the radiative properties depend on the observation angle) and a geometric (since it changes the equivalent area sensed by the sensor) effect. The latter is by far the most important in the presence of heterogeneous scenes and with a varying degree of beamfilling. In our tests, the viewing angle was randomly varied around 53.1° (from 45.5° to 61°). Peak deviations (up to ± 20 K at 85 GHz) are observed near cloud edges, where completely different structures (rain/no-rain or ice/no-ice) are covered by the radiometer footprint. The TB deviations in Fig. 1(e) indicate an important effect at 85 and even at 37 GHz. Biases show bizarre features at various frequencies with 10- and 19-GHz channels showing opposite trends (negative-to-positive) with respect to 37 and 85 GHz. This is due to the fact that changing the viewing angle results in different apparent equivalent areas of cloud and the rainy region. This results in an overall heating at rain-emission-related frequencies, and cooling at scattering-related frequencies. At low frequencies, clear sky regions are biased (up to 1.5 K), due to the variation of the optical path with the viewing angle, as well as from the different response of the surface.

Antenna Beamwidth: The brightness temperatures are computed at model resolution and successively filtered by a two-dimensional (2-D) antenna gain function. The antenna radiation pattern is simulated through a bivariate Gaussian function, where the half-power beamwidth equals the nominal footprint size of the antenna at that frequency in the cross/along-track direction. Sidelobe effects have been neglected. The resulting effect of antenna beamwidth instabilities is proportional to the half-power beamwidth (i.e., to the footprint size), and it therefore decreases with frequency. This analysis depends on the size of the targeted area with respect to the beam size and thus it substantially reflects the beamfilling problem (see [35]) and is more pronounced in heterogeneous scenes.

In our test, we varied the antenna aperture up to a maximum of 15%. The results [see Fig. 1(f)] show an effect only at 10 GHz, because of the very large footprint area of this channel (approximately 60 km $\times$ 40 km). It should be noted that this experiment may be underestimating the general problem due to the large dimension of the simulated hurricane. If similar tests are carried out for smaller-scale convective cells more extreme TB-variations would be obtained.

C. Sensitivity Analysis of Model Approximations

In addition to the above-mentioned parameters, the impact of the following approximations has been considered:

- 3-D versus one-dimensional (1-D) Radiative transfer model;
- presence versus absence of melting particles;
- spherical versus nonspherical particles.

Indeed, the interest in this further analysis stems from the fact that current forward-radiation models tend to neglect the 3-D radiative effects, the impact of melting layer and the role of nonspherical particles. Once the latter refined parameterizations were included, a sensitivity analysis of their uncertainties—similar to what previously shown—would be appropriate (e.g., see [40] for the melting model).

Radiative Transfer Model: Radiative transfer models have reached a high degree of accuracy. The most refined RT models are capable of describing the full 3-D paths followed by the radiation inside a complete 3-D cloud structure. However, these models are computationally heavy, and rely fully on the macrophysical structure of the cloud-model simulation. As introduced in Section II, we have adopted a "pseudo-3-D" RT scheme (called the "slanted-path plane parallel"), in which plane-parallel RT calculations are performed along a slanted profile in the direction of observation of the radiometer. The method is computationally efficient and provides a first-order approximation to 3-D RT; however it only accounts for radiative fluxes within the 1-D column. The performance of the slanted-path plane-parallel RT approximation has been investigated by several authors ([21] and [36] among many others). They generally agree that the errors are limited to a few Kelvin on average scenes, even though local values may be important

[11]We obtained that the surface characteristics have almost no influence at 37 GHz, while at 10 GHz it is relevant even for very high rainfall rates (RR $>$ 50 mm/h).

in case of large horizontal gradients (e.g., at the cloud edges) (see [37] and [38]) and at higher frequencies.

We have analyzed the errors due to a pseudo-3-D approximation on a pixel-by-pixel basis by comparing the upwelling brightness temperatures to those obtained from using a 3-D backward Monte Carlo method [21]. The average errors are generally lower than a few Kelvin at TMI resolution and at TMI frequencies but local values increase where large cloud inhomogeneities occur. Maximum TB differences of 13 K were found at 85 GHz, which is consistent with [38], who suggested that 1-D TB calculations at 85 GHz in strong scattering regions should be regarded with caution.

Melting Phase: Melting hydrometeors have different radiative properties with respect to homogeneous liquid or frozen particles. This is often observed in stratiform clouds with weak updrafts where frozen precipitation particles sediment below the freezing level over large areas. While this process is very well captured by radar measurements,[12] less research has been carried out on the passive microwave signatures (see [39]–[42]) in the presence of absorbing and scattering cloud layers above the melting layer. Literature generally reports TB heating at all frequencies, due to the abrupt increase in absorption/emission properties of the partially melted, large frozen particles. This heating generally decreases with frequency because at high frequencies the presence of frozen as well as supercooled rain particles aloft would eventually obscure the signal. From 3-D simulations, [40] and [41] found TB increases as large as 8 K at the lower frequencies (10 and 19 GHz) over ocean. Bauer *et al.* [39] examined different permittivity models of melting particles in a 2-D cloud model, obtaining TB differences that vary enormously with the cloud structure under examination and with the melting and size distribution model adopted. Remarkably, including the melting effect may in some cases (peak graupel concentrations) induce slight cooling at low frequencies, while strong heating is found at 37 GHz. Olson *et al.* [42] found TB increases as large as 43 K at 10 GHz and 10 K at 85 GHz at 1-km resolution. The numbers drastically decrease if the true TMI resolution is accounted for (16 and 9 K, respectively).

For modeling melting particles within 3-D mesoscale cloud dynamical models, the explicit calculation of latent heat fluxes is required. However, since only the output of the cloud-model simulation is available, a simpler approach was chosen (as in [40] and [41]). The melting model has been only applied where the Hurricane Bonnie simulation indicated the presence of melting graupel/snow/aggregates, and only for stratiform precipitation.[13] For computing the radiative properties of single particles, the permittivity model in [43] has been used. From our calculations at TMI resolution, we found heating as large as 1.8 and 3.5 K (at 10 and 37 GHz, respectively) and cooling as low as -1 K at 85 GHz.

Particle Shapes: Hydrometeors are not spherical: rain drops become elliptic and even bean-shaped; graupel particles can be considered conical with upward directed apexes; snowflakes and ice crystals show complex and a largely variety of shapes [45]. If particles are nonspherical, their radiative signature depends on the observation geometry and on the orientation and shape of the particles. The most remarkable effect is that nonsphericity generates polarization (depending on frequency, viewing angle, cloud structure, and surface conditions; for a complete review on the subject, see [46]). An important indicator of the nonsphericity of hydrometeors is the presence of strongly polarized TBs over surfaces that reflect radiation nearly isotropically and unpolarized, i.e., rough land surfaces. Literature reports polarization differences up to 13 K at 85 GHz and 7 K at 37 GHz, but these values depend on sensor resolution and on the cloud system under investigation [46]. The polarization difference generated by rain drops is expected to be (at most) a few degrees at TMI viewing angle. For ice particles, the effect may be more significant and depend on the assumptions made on the characteristics of the particles themselves [34], [47] as well as on their orientation.

In our RT scheme, we have assumed spherical hydrometeors and made use of Mie theory for computing their scattering properties. The errors introduced by this approximation should be, in principle, evaluated by running a polarized RT model (e.g., [34]) and by computing the TB differences with respect to the corresponding unpolarized TBs. However, a detailed analysis is beyond the scope of the present work. Since we are mostly interested in evaluating the potential overall effect at the sensor level, we introduced perturbations to the sphericity standard assumption. The sensitivity of particle emission/scattering to particle shapes was expressed in terms of the variation of the volumetric Mie optical parameters proportional to variations in equal-volume sphere particle size. The Mie parameters of every cloud grid box have been randomly perturbed up to a rainfall rate-dependent threshold (always within approximately 10% of the value itself) derived from [48] for uniformly oriented, oblate particles at 50° viewing angle. The RT scheme has been run over the perturbed 3-D structure and the TB deviations from the standard database have been considered to account for the average error induced by the presence of nonspherical particles. From this test, we have obtained polarization differences not larger than a few Kelvin at all frequencies. The errors are randomly distributed according to the rain and ice columnar contents, and show peak values between 1 K at 10 GHz and 4 K at 37 GHz. Surprisingly, the most important effect is found at 37 and 19 GHz.

III. Error Budget

A synoptic visualization of the results for the assumed values of the perturbation factors (as indicated in Table I) is presented in Fig. 2, where the impact of the different parameters for the various frequencies is quantified in terms of error variances. A rainfall threshold of 0.2 mm/h (at 37-GHz TMI resolution) has been used for screening out clear-sky pixels.[14]

From our analyses, agreement was found with Panegrossi *et al.* [22] about the size spectra of both rain and precipitating ice particles being one of the most influencing factors for the upwelling radiances. This effect is dominant at 19 GHz and especially at 37 GHz. Ice particle modeling errors dominate at 37 GHz and especially at 85 GHz. The effect of sea surface wind

[12]This is the well-known "brightband" effect.

[13]The stratiform/convective classification is accomplished on the basis of the vertical wind speed (1 m/s being the threshold for convective precipitation, as from [44]), even if the UW-NMS simulation indicates the presence of melting particles even in regions of strong updrafts (>10 m/s).

[14]The database classification has obviously an important impact on the obtained error covariance matrix. In principle, different error covariance matrices should be associated to every CRD class.

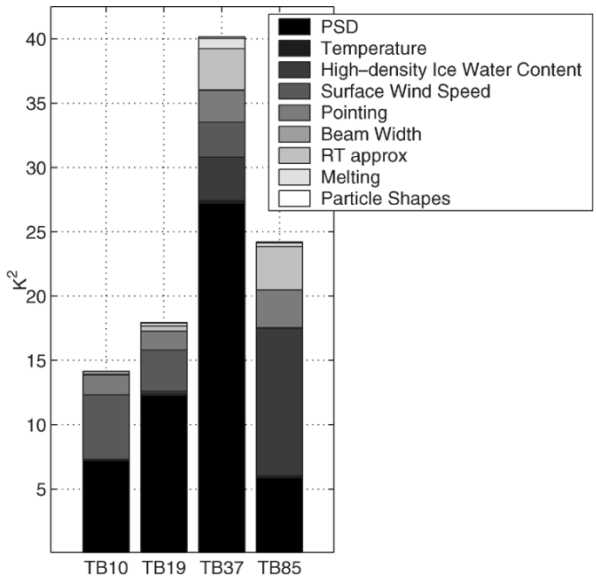

Fig. 2. Model error autocovariances at four TMI frequencies and at TMI resolutions. The contribution of the different parameters is evidenced by different shaded blocks.

TABLE II
(a) CLOUD-RADIATION DATABASE MODELING ERROR COVARIANCE MATRIX. (b) MODEL MEAN ERRORS MATRIX

	TB10V	TB10H	TB19V	TB19H	TB37V	TB37H	TB85V	TB85H
TB10V	8.3	11.2	5.2	6.7	4.9	5.4	0.9	1.0
TB10H	11.2	17.8	5.2	8.1	4.5	5.5	0.3	0.3
TB19V	5.2	5.2	15.	15.7	21.1	21.2	8.0	7.9
TB19H	6.7	8.1	15.7	18.1	20.6	21.6	7.4	7.4
TB37V	4.9	4.5	21.1	20.6	44.	43.1	23.	22.7
TB37H	5.4	5.5	21.2	21.6	43.1	43.8	22.1	22.2
TB85V	0.9	0.3	8.	7.4	23.	22.1	30.5	29.9
TB85H	1.	0.3	7.9	7.4	22.7	22.2	29.9	30.1

(a)

	TB10V	TB10H	TB19V	TB19H	TB37V	TB37H	TB85V	TB85H
Mean Values	3.0	3.4	2.2	1.8	6.4	5.4	5.2	4.4

(b)

speed is only important at 10 and 19 GHz. Pointing instabilities are sensed at all frequencies. RT approximations play a significant effect at 37 and 85 GHz. The most striking features from Fig. 2 are: 1) the importance of PSD modeling at all frequencies (even at 10 GHz) and 2) the very high degree of uncertainty of the 37-GHz channel, especially related to the unknown parameterization of PSDs and of frozen hydrometeors. As a matter of fact, this TMI channel carries a large amount of information for quantitative estimations of rainfall due to its high sensitivity and its large dynamic range. However, this potential is dramatically reduced by the actual uncertainties in the interpretation of the measurements. Thus, this channel should be inserted very carefully in the inversion process.

It is important to notice that these results have been obtained at TMI resolutions: this means that the detailed behavior of radiation at these frequencies is filtered through the antenna weighting function. When changing the resolution, results may be different. This is outlined in the Appendix.

A. Database Error Covariance Matrix

Table II(a) shows the complete error covariance matrix obtained for our cloud-radiation database. The values on the diagonal correspond to the error variances of Fig. 2. Horizontal (H) and vertical (V) polarizations are highly correlated for the same frequency with correlation coefficients ranging from 0.97 at 10 GHz to 0.996 at 85 GHz. $\mathbf{M_{CRD}}$ is symmetric but not diagonal. This means that errors for the different channels are not mutually uncorrelated as it is often assumed. In particular, the errors at 37 GHz show correlation with those at both 19 (unpolarized correlation coefficient $\rho_{19-37} = 0.84$) and 85 GHz ($\rho_{19-37} = 0.65$), while the errors at 10 GHz appear anticorrelated with all the other channels ($\rho_{10-19} = -0.19$, $\rho_{10-37} = -0.58$, and $\rho_{10-85} = -0.93$). The error standard deviation $\boldsymbol{\sigma}_{\mathrm{CRD}}$ (the square root of the elements on the diagonal of the matrix, with unpolarized values of 3.6, 4.0, 6.6, and 5.5 for the four frequencies) determines the intrinsic limitation in the capability of resolving between adjacent TB pixels of the CRD. The quantity $\boldsymbol{\sigma}_{\mathrm{CRD}}$ determines the dimensions of the elementary pixel in the eight-dimensional (8-D) space of the simulated TBs and can be considered as a measure of CRD resolution. Finally, it is important to notice that non-zero mean model errors have been obtained, due to the nonlinearities in the geophysical parameter–TB relationship. Table II(b), shows that biases are nonnegligible at all frequencies, especially at 37 GHz (we obtained from 2 K at 19 GHz to 6 K at 37 GHz). This result is in contrast with the usual assumption of Gaussian zero-mean errors (e.g., see [13]).

It must be recognized that a very critical assumption has been made on the mutual independence of the single parameters, whose effects have been accounted for separately (the overall effect has been computed by adding the error covariances due to the single parameters). This is not necessarily correct. For example, the melting phase is related to the quantity and size distribution of ice particles, the PSDs of graupel and rain are correlated, and so on. However, all this information should be derived through direct coupling with the cloud-model simulation itself, the complete analysis requiring time- and computer-consuming additional cross-tests. The error covariance matrix, completed with a white instrumental noise, accounts for the overall error variance to be inserted within the inversion scheme.

B. Database Ambiguity

The term *database ambiguity* comes from [5], and it describes the problem of the nonunique relationship between TBs and precipitation parameters. Different profiles can generate similar TB vectors that cannot be distinguished as long as they remain within the CRD resolution distance $\boldsymbol{\sigma}_{\mathrm{CRD}}$ determined by the $\mathbf{M_{CRD}}$ matrix. Fig. 3 shows the relative dispersion of surface rainfall rate, columnar liquid rain, and columnar ice as function of the mean values. The relative uncertainty of ice and rain water

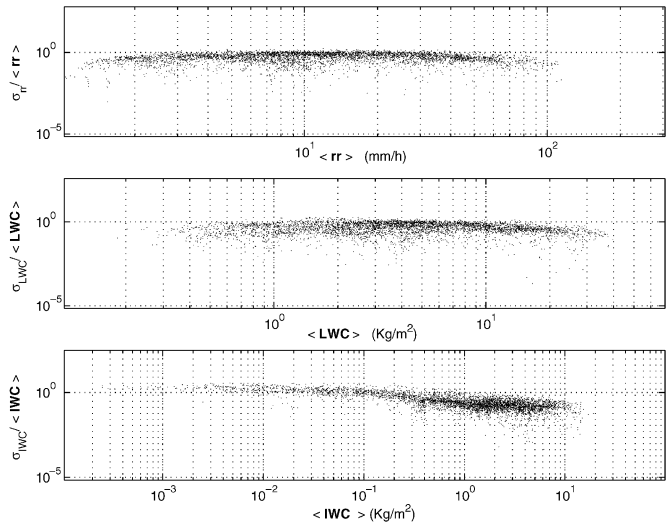

Fig. 3. Database ambiguity. Normalized error standard deviations as functions of the mean values for (from top to bottom) surface rainfall rate (millimeters per hour), columnar rain (kilograms per square meter), and columnar graupel (kilograms per square meter).

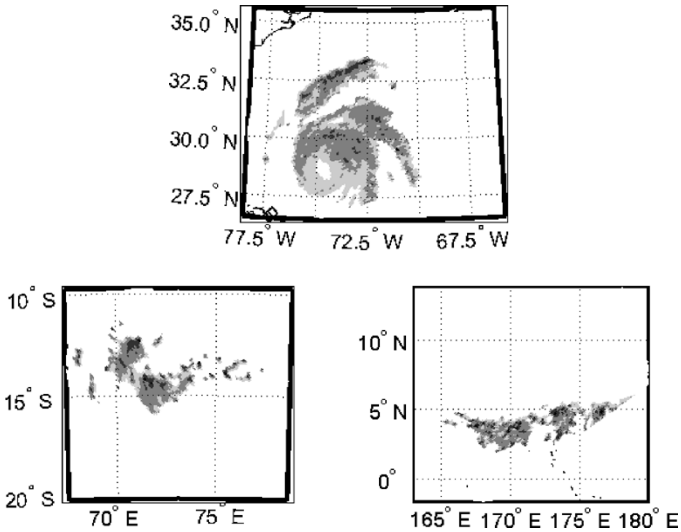

Fig. 4. Database matching maps for TMI granules 4267, 11 938, and 18 023. The different shaded pixels represent the different degrees of matching. Light gray pixels are completely overlapped in the simulation manifold [DMI(1)]. Gray pixels correspond to DMI(2), whilst the very dark dots correspond to DMI(3). Unmatched pixels are not clearly visible in the maps (they constitute only 1% of the overall dataset).

contents strongly decreases with the mean values while for rain rates it is always larger than 1.

IV. Comparison With Measurements

The realistic appearance of a cloud-radiation database, as well as its potential adequateness for interpreting given meteorological events, should be evaluated with respect to the measurements. The necessity of this intercomparison has been stressed by several authors, both in terms of TBs [22] as in terms of principal components [5], [6]. This comparison should indicate the capability of the cloud-radiation database in reproducing the radiative features of the chosen events both in terms of TB distributions at every single frequency as well as in the relationships among the different channels.

A. Database Matching Index

In this work the overlap between the manifold of the simulated TBs and that of the measurements is quantified with respect to the CRD resolution $\boldsymbol{\sigma}_{\mathrm{CRD}}$, which is assumed as a reference distance (in the 8-D space of the TMI channels, since the 21.3-GHz channels were omitted). When comparing the simulated with the measured data also the measurement noise shall be taken into account. Therefore, the reference distance can be corrected with the measurement noise which leads to $\boldsymbol{\sigma}_{\mathrm{ref}} = (\boldsymbol{\sigma}^2_{\mathrm{CRD}} + \boldsymbol{\sigma}^2_{\mathrm{MEAS}})^{1/2}$, where $\boldsymbol{\sigma}_{\mathrm{MEAS}}$ is assumed equal to 1.5 K at 85 GHz and 1 K for all other frequencies (see [13]).

For every measured CRD pixel represented by a multichannel TB vector $\mathbf{P_{MEASi}}$, the distance Δ_i from the closest pixel $\mathbf{P_{SIM\ j}}$ of the simulated database is computed and compared to $\boldsymbol{\sigma}_{\mathbf{ref}}$: if $\Delta_i \leq \boldsymbol{\sigma}_{\mathbf{ref}}$, then $\mathbf{P_{MEASi}}$ is considered to be represented within the simulated manifold. The ratio between the number of "represented" pixels (N_σ) and the total number of observed pixels (N_{MEAS}) is used for quantifying the matching between the two manifolds and is called a database matching index, DMI from now on. Note that this is a refinement of the DMI already introduced in [16]. This requirement can be relaxed by defining Δ_i as a step function of $\boldsymbol{\sigma}_{\mathbf{ref}}$, i.e., considering

$$\Delta_i \leq n\sigma_{\mathrm{ref}} \tag{2}$$

with $n = 1, 2, 3, \ldots, n_{\mathrm{MAX}}$ and n_{MAX} defined according to the given requirements. Through (2), the matching between the TB simulations and measurements may be evaluated at different degree thresholds. Then we can define DMI as

$$\mathrm{DMI}(n) = \frac{N_{n\sigma}}{N_{\mathrm{MEAS}}} \tag{3}$$

where $N_{n\sigma}$ is the number of pixels showing overlapping at distances $\Delta_i \leq n\boldsymbol{\sigma}_{\mathbf{ref}}$. Using this notation, the DMI previously introduced corresponds to DMI(1). Successive levels would indicate that less overlap is present. DMI(n_{MAX}) expresses the percentage of pixels having *at least* the n_{MAX} degree of coverage within the simulated manifold.

B. Application to TMI Data

Three different case studies have been selected for the evaluation of the CRD: 1) a tropical cyclone (Hurricane Bonnie) which overpassed the coast of South Carolina on August–September 1998; 2) a tropical storm ("Hurricane" Astrid) which devastated the coasts of Mozambique on December 1999; 3) a tropical front which occurred over the Pacific Ocean in January 2001. The Hurricane Bonnie case is, of course, of particular interest since our CRD is composed by a simulation designed for the same event.

Fig. 4 shows the resulting database matching index maps for the three cases under examination in terms of three different degrees of matching $(n_{\mathrm{MAX}} = 3)$. The maps provide a valuable tool for understanding the regions of mismatch between the simulated and the measurements manifolds, setting apart random problems and systematic mismatches that could be due to given

TABLE III
DMIs OBTAINED FOR THREE DIFFERENT CASE STUDIES (INDICATED IN THE RIGHT COLUMN) AND FOR DIFFERENT VALUES OF THE TB ERROR AUTOCOVARIANCES (INDICATED IN THE FIRST COLUMN). IN THE LAST TWO TESTS, VALUES AS FROM TEST2 AND TEST4 OF [13] ARE USED, CORRESPONDING TO (FROM 10–85 GHz): 1., 5.3 (12.9 AT H pol), 2.6, AND 6.7 K AND TO 1., 5.3 (12.9 AT H pol), 2.6, AND 42.2 K, RESPECTIVELY. VALUES EXCEEDING THE REFERENCE ONE ARE IN BOLD

Sigma	DM I(1)	DMI(2)	DMI(3)	TMI case
σ_{CRD}+ noise	0.44	0.96	0.99	Granule 4267
	0.33	0.86	0.99	Granule 11938
	0.34	0.84	0.98	Granule 18023
σ =3K+ noise	0.18	0.64	0.92	Granule 4267
	0.12	0.51	0.82	Granule 11938
	0.15	0.52	0.79	Granule 18023
σ =5K+ noise	0.41	0.92	0.99	Granule 4267
	0.32	0.81	0.98	Granule 11938
	0.34	0.79	0.97	Granule 18023
σ =6K+ noise	**0.53**	**0.97**	**1.00**	Granule 4267
	0.41	**0.92**	**0.99**	Granule 11938
	0.43	**0.88**	**0.98**	Granule 18023
σ T4 from [13] + noise	0.13	0.60	0.89	Granule 4267
	0.11	0.46	0.76	Granule 11938
	0.08	0.47	0.74	Granule 18023
σ T2 from [13] + noise	0.05	0.44	0.71	Granule 4267
	0.03	0.32	0.55	Granule 11938
	0.04	0.33	0.58	Granule 18023

micro/macrophysical characteristics. In this case, for instance, they show how a consistent portion of an events which is not adequately represented within the hurricane simulation, is mostly located near cloud edges and small convective cells. Table III indicates the corresponding DMIs (1), equal to 0.44, 0.33, and 0.34, respectively. When considering DMIs up to the third level values up to 0.99, 0.99, and 0.98 are obtained. The largest values are always obtained for the Hurricane Bonnie case, a fact which is most likely related to the fact that our database contains the simulation dedicated to the same event. The data fitting can be considered remarkable, given the limited dimensions of the CRD.

The representativeness of the computed $\boldsymbol{\sigma}_{\mathrm{CRD}}$ with respect to other criteria has been evaluated by choosing other values, either constant with frequency (i.e., 3, 5, or 6 K for all channels) or the ones used within specific tests in [13]. All the tested values lead to DMIs smaller than the reference ones, except for the $\boldsymbol{\sigma}_{\mathrm{CRD}} = 6$ K case that corresponds to values larger than the reference $\boldsymbol{\sigma}_{\mathrm{CRD}}$ for all frequencies except at 37 GHz. As obvious, this very poor CRD resolution turns out into very large database ambiguities especially associated to rain rate.[15]

In conclusion, the computed $\boldsymbol{\sigma}_{\mathrm{CRD}}$ seems to provide the best database performances with respect to the other tested σ values, by providing the smallest dispersion associated to the best agreement with the measurements. Of course, it must be noticed that the CRD capability in reproducing the radiative signatures of a given meteorological event is a necessary but not sufficient condition to assess the CRD representativeness. It does not imply the reliability of the microphysics associated to the TBs, which depends on the cloud-model simulation itself and would require *in situ* measurements to be checked.

[15]If we quantify the uncertainty in terms of the ratio between the standard deviation and the mean columnar for the various hydrometeors (as illustrated in the y axes of Fig. 3), we obtain, for columnar rain, average values of 0.33 for the $\sigma\mathrm{CRD}$ case and 0.38 when using $\sigma = 6$ K. For columnar ice, we pass from 0.28 to 0.29: the difference is not remarkable, since the values used for the higher frequencies are not very different.

V. CONCLUSION

Model error covariance matrices are needed within both rainfall retrieval algorithms and numerical weather data assimilation for quantifying the degree of accuracy of the simulated *a priori* information. Bayesian physically based precipitation retrieval algorithms make use of model-derived cloud-radiation databases as *a priori* information. In this work, we have built a "generalized" cloud-radiation database composed of simulated radiances (and corresponding precipitation structures) and of the associated error covariance matrix. The matrix has been generated by means of TB-sensitivity tests with respect to different reference parameters (i.e., variable drop size distributions, temperature profiles, ice water contents, sea surface wind speeds, viewing angles, antenna beam sizes, the radiative transfer approximation, the presence of melting particles, and particles shape). The tests have been carried out on the output of the cloud-model simulation. In the absence of cloud-model-derived detailed information, simplistic assumptions have been made on parameter perturbations being mutually independent and randomly distributed. Deeper analyses should imply a strict coupling between the radiative and the dynamical model since other error sources—linked to the dynamical simulation itself—should be considered. Also, experiments were confined only to a snapshot of a hurricane simulation, so that the results are not applicable to different kinds of weather events. The invariance of the error covariance matrix for similar events should be investigated. In spite of the above-mentioned limitations, however, the tests show interesting results about the relative importance of the various uncertainties for the different channels and allow interesting comparisons among the various parameters (in terms of impact on the TBs). From our numerical experiments it has turned out that the size spectra of both rain and graupel are the most influencing factors for the upwelling radiances, especially at 19 and 37 GHz. Sea surface wind speed may play a very important role at 10 GHz, while ice particle modeling uncertainties are dominant at 37 and especially at 85 GHz. In summary, it has been obtained that the TMI 37-GHz channels are characterized by a very high degree of uncertainty, mainly determined by the high-density ice particles modeling (size spectrum, nonsphericity, amounts, and composition).

From the error budget, a final overall error standard deviation has been computed for each channel. Unpolarized standard deviations $(\boldsymbol{\sigma}_{\mathrm{CRD}})$ as large as 3.6, 4, 6.6, and 5.5 K have been obtained at 10, 19, 37, and 85 GHz , respectively. $\boldsymbol{\sigma}_{\mathrm{CRD}}$ was used for assessing the ambiguity of the database, as well as to quantify the agreement between the simulated radiances and the observations. The simulated TBs and the impact of the associated modeling error covariance matrix have been examined with respect to actual TMI measurements for three different case studies (i.e., TMI passages over Hurricane Bonnie—which is the same event simulated by the model; over a tropical storm and an oceanic front). A disagreement is evident when performing an 8-D analysis in terms of database matching indexes: three times the basic noise figure is generally required for obtaining a complete overlapping of the measurements. DMIs change with the meteorological event under observation, but the best performances are always obtained for the hurricane case.

Interesting results have also emerged when the spatial resolution of the simulated radiometer was accounted for. The impact

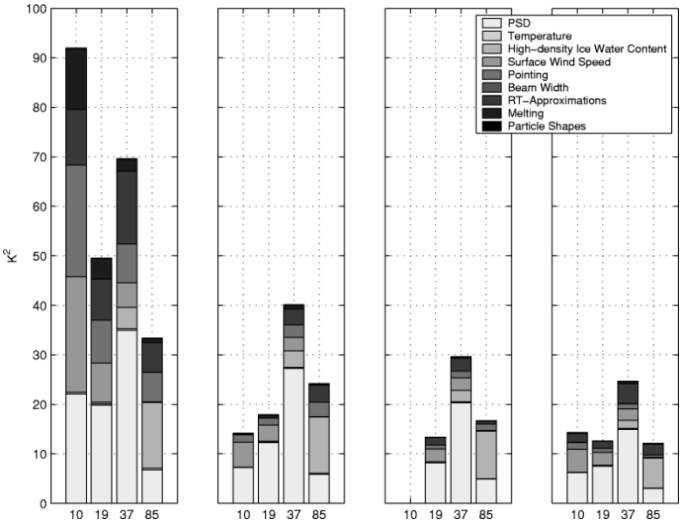

Fig. 5. Unpolarized error variances at four TMI frequencies and at different resolutions (from left to right: model—i.e., 2.5 km, TMI, SSMI, and 60 × 60 km). The contribution of the different parameters is evidenced separately.

of the sensor spatial resolution characteristics tends to dominate. On one hand, results for TMI and SSM/I resolutions show similar trends concerning the impact of the different geophysical parameters at the various frequencies. On the other hand, at the model resolution (here 2.5 km, comparable or larger than what airborne sensors can operate), the results are completely different: the 10-GHz channel shows large sensitivity to particles size distributions as well as to RT approximations, revealing that much of the claimed robustness for this channel is principally due to the very low resolution currently obtained with satellite-based sensors.

The present study should be considered an initial step toward a systematic error/uncertainty investigation within Bayesian precipitation inversion schemes. Future work will be devoted to extend our cloud-radiation database to other rain cloud simulations in various meteorological and climatological scenarios, in order to achieve more representativeness. In this respect, error covariance matrices derived from numerical simulations of different precipitation systems could be analyzed, compared, and added to the present one, with the final purpose of obtaining a comprehensive library of matrices/databases for inversion purpose. From the point of view of retrieval algorithms, this would be of great importance, since it would reduce the number of events to be simulated and would extend the applicability of given cloud-radiation databases.

APPENDIX
EVALUATING CLOUD-RADIATION DATABASE MODELING ERRORS AT VARYING SPATIAL RESOLUTIONS

The database modeling error covariance matrix in Table II and the autocovariances shown in Fig. 2 have been computed at TMI resolution. However, when computed at different resolutions, they show very different behaviors. This is evident from Fig. 5, where error variances at the resolution of the cloud model (2.5 km), at SSM/I[16] and at 60-km resolution are shown. In Fig. 5(a), error variances at model resolution are shown. These results may be considered the most representative of the pure "physics," being not affected by any beamfilling problem (at least with respect to our source cloud model). In Fig. 5(d), a very low resolution case is shown (60 × 60 km for all channels): the smoothing decreases the uncertainties by more than 80%, but the relationships among the various channels have not been altered by the antenna footprints. This is not true for the cases of the TMI and SSM/I resolution in Fig. 5(b) and (c).

The impact of PSDs, surface conditions, RT approximations, pointing errors, and melting is dominant at 10 GHz as well as at 19 GHz. At 37 GHz, PSD and RT approximations play the most important role. RT approximations and high-density ice water contents are the main factors at 85 GHz. At TMI resolution, the largest uncertainty is at 37 GHz (for more details about the TMI case, see comments about Fig. 2). For the SSM/I, the resulting trends are similar to the TMI case. The overall amounts increase with resolution, ranging from 22 K^2 at 37 GHz (12 K^2 at 85 GHz) at 60-km resolution [Fig. 5(d)] to 97 K^2 (47 K^2 at 85 GHz) at 2.5-km resolution [Fig. 5(a)]. The most interesting feature is the changing trend for the different frequencies. The tendency—already observed at TMI resolution—of the maximum errors being at 37 GHz is confirmed at all resolutions. An exception is present at model resolution when the 10-GHz frequency shows unexpected huge errors as large as 100 K^2. This behavior seems mostly related to the extraordinary impact of the pointing errors (which reduce by almost 15% when lowering the resolution) near rain cell edges. We also notice that the relative smoothness of the 10-GHz channel TBs with respect to the other channels is exclusively due to the low spatial resolution on TRMM. In fact, if all uncertainties are computed at the same resolution, this channel shows as much instability (due to the PSD modeling as well as to the surface or to the RT approximations) as the other channels.

[16]SSM/I footprints are roughly proportional—but larger—than TMIs.

ACKNOWLEDGMENT

The authors wish to thank G. Tripoli and G. Panegrossi (University of Wisconsin) for providing the Hurricane Bonnie simulation and for profitable interactions.

REFERENCES

[1] J. R. Simpson, C. Kummerow, W. K. Tao, and R. F. Adler, "On the Tropical Rainfall Measuring Mission (TRMM)," *Meteorol. Atmos. Phys.*, vol. 60, pp. 19–36, 1996.

[2] T. Wilheit, R. Adler, S. Avery, E. C. Barrett, P. Bauer, W. Berg, A. Chang, J. Ferriday, N. Grody, S. Goodman, C. Kidd, D. Kniveton, C. Kummerow, A. Mugnai, W. Olson, G. Petty, A. Shibata, E. A. Smith, and R. W. Spencer, "Algorithms for the retrieval of rainfall from passive microwave measurements," *Remote Sens. Rev.*, vol. 11, pp. 163–194, 1994.

[3] E. A. Smith, J. Lamm, R. Adler, J. Alihouse, K. Aonashi, E. Barrett, P. Bauer, W. Berg, A. Chang, R. Ferraro, J. Ferriday, S. Goodman, N. Grody, C. Kidd, C. Kummerow, G. Liu, F. S. Marzano, A. Mugnai, W. Olson, G. Petty, A. Shibata, R. Spencer, F. Wentz, T. T. Wilheit, and E. Zipser, "Results of WetNet PIP-2 projects," *J. Atmos. Sci.*, vol. 55, pp. 1483–1536, 1998.

[4] C. Kummerow, Y. Hong, W. S. Olson, S. Yang, R. F. Adler, J. Mc Collum, R. Ferraro, G. Petty, D. B. Shin, and T. T. Wilheit, "The evolution of the Goddard profiling algorithm (GPROF) for rainfall estimation from passive microwave sensors," *J. Appl. Meteorol.*, vol. 40, pp. 1801–1820, 2001.

[5] P. Bauer, "Over-ocean rainfall retrieval from multisensor data of the tropical rainfall measuring mission. Part I: Design and evaluation of inversion databases," *J. Atmos. Oceanic Technol.*, vol. 18, no. 8, pp. 1315–1330, 2001.

[6] G. W. Petty, "Physical and microwave radiative properties of precipitating clouds. Part 1: Principal component analysis of observed multichannel microwave radiances in tropical stratiform rainfall," *J. Appl. Meteorol.*, vol. 40, pp. 2105–2129, 2001.

[7] A. Tassa, S. Di Michele, E. D'Acunzo, C. Accadia, S. Dietrich, A. Mugnai, F. Marzano, G. Panegrossi, and L. Roberti, "Analysis of TRMM observations of heavy precipitation events," presented at the *Microwave Radiometry and Remote Sensing of the Earth's Surface and Atmosphere, 6th Specialist Meeting*, 1999, pp. 371–377.

[8] E. A. Smith, X. Xiang, A. Mugnai, and G. J. Tripoli, "Design of an inversion-based precipitation profile retrieval algorithm using an explicit cloud model for initial guess microphysics," *Meteorol. Atmos. Phys.*, vol. 54, pp. 53–78, 1994.

[9] C. Kummerow, W. S. Olson, and L. Giglio, "A simplified scheme for obtaining precipitation and vertical hydrometeor profiles from passive microwave sensors," *IEEE Trans. Geosci. Remote Sens.*, vol. 34, no. 5, pp. 1213–1232, Sep. 1996.

[10] J. L. Haferman, E. N. Anagnostou, D. Tsintikidis, W. F. Krajewski, and T. F. Smith, "Physically based satellite retrieval of precipitation using a 3-D passive microwave radiative transfer model," *J. Atmos. Oceanic Technol.*, vol. 13, no. 4, pp. 832–850, 1996.

[11] M. Grecu and E. M. Anagnostou, "Overland precipitation estimation from TRMM passive microwave observations," *J. Appl. Meteorol.*, vol. 40, pp. 1367–1380, 2001.

[12] F. S. Marzano, A. Mugnai, G. Panegrossi, N. Pierdicca, E. A. Smith, and J. Turk, "Bayesian estimation of precipitating cloud parameters from combined measurements of spaceborne microwave radiometer and radar," *IEEE Trans. Geosci. Remote Sens.*, vol. 37, no. 1, pp. 596–613, Jan. 1999.

[13] S. Di Michele, A. Tassa, A. Mugnai, F. S. Marzano, P. Bauer, and J. P. V. Baptista, "Bayesian algorithm for microwave-based precipitation retrieval: Description and application to TMI measurements over ocean," *IEEE Trans. Geosci. Remote Sens.*, vol. 43, no. 4, pp. 778–791, Apr. 2005.

[14] A. C. Lorenc, "Analysis methods for numerical weather prediction," *Q. J. R. Meteorol. Soc.*, vol. 112, pp. 1177–1194, 1986.

[15] P. Bauer, J. F. Mahfouf, W. S. Olson, F. S. Marzano, S. Di Michele, A. Tassa, and A. Mugnai, "Error analysis in rainfall retrieval for variational data assimilation," *Q. J. R. Meteorol. Soc.*, vol. 128, pp. 2129–2144, 2002.

[16] A. Tassa, S. Di Michele, A. Mugnai, F. S. Marzano, and J. P. V. Poiares Baptista, "Cloud model-based Bayesian technique for precipitation profile retrieval from the Tropical Rainfall Measuring Mission Microwave Imager," *Radio Sci.*, vol. 38, no. 4, p. 8074, 2003.

[17] P. Bauer, E. Moreau, and S. DiMichele, "Hydrometeor retrieval accuracy from microwave window and sounding channel observations," *J. Appl. Meteorol.*, vol. 44, pp. 1016–1032, 2005.

[18] S. Di Michele, F. S. Marzano, A. Mugnai, A. Tassa, and J. P. V. Poiares Baptista, "Physically based statistical integration of TRMM microwave measurements for precipitation profiling," *Radio Sci.*, vol. 38, no. 4, p. 8072, 2003.

[19] G. Panegrossi, A. Tassa, S. Di Michele, G. J. Tripoli, A. Mugnai, and E. A. Smith, "Using TRMM observations to improve numerical simulations of precipitation within tropical cyclones," in *Proc. Symp. Precipitation Extremes: Prediction, Impacts, and Responses*, 2001, pp. 324–326.

[20] G. J. Tripoli, "An explicit three-dimensional nonhydrostatic numerical simulation of a tropical cyclone," *Meteorol. Atmos. Phys.*, vol. 49, pp. 229–254, 1992.

[21] L. Roberti, J. Haferman, and C. Kummerow, "Microwave radiative transfer through horizontally inhomogeneous precipitating clouds," *J. Geophys. Res.*, vol. 99, pp. 16 707–16 718, 1994.

[22] G. Panegrossi, S. Dietrich, F. S. Marzano, A. Mugnai, E. A. Smith, X. Xiang, G. J. Tripoli, P. K. Wang, and J. P. V. Poiares Baptista, "Use of cloud model microphysics for passive microwave-based precipitation retrieval: Significance of consistency between model and measurement manifolds," *J. Atmos. Sci.*, vol. 55, pp. 1644–1673, 1998.

[23] D. LeMaire, P. Sobieski, and A. Guissard, "Full-range sea surface spectrum in nonfully developed state for scattering calculations," *IEEE Trans. Geosci. Remote Sens.*, vol. 37, no. 2, pp. 1038–1051, Mar. 1999.

[24] N. Viltard, C. Kummerow, W. S. Olson, and Y. Hong, "Combined use of the radar and radiometer of TRMM to estimate the influence of drop size distribution on rain retrievals," *J. Appl. Meteorol.*, vol. 39, pp. 2103–2114, 2000.

[25] J. S. Marshall and W. McK. Palmer, "The distribution of raindrops with size," *J. Meteorol.*, vol. 5, pp. 165–166, 1948.

[26] C. W. Ulbrich, "Natural variations in the analytical form of the raindrop size distribution," *J. Clim. Appl. Meteorol.*, vol. 22, pp. 3452–3459, 1983.

[27] P. T. Willis and P. Tattelmenn, "Drop-size distributions associated with intense rainfall," *J. Appl. Meteorol.*, vol. 28, pp. 3–15, 1989.

[28] J. Testud, S. Oury, R. A. Black, P. Amayenc, and X. Dou, "The concept of "normalized" distribution to describe raindrop spectra: A tool for cloud physics and cloud remote sensing," *Appl. Meteorol.*, vol. 40, pp. 1118–1140.

[29] R. A. Houze, P. V. Hobbs, P. H. Herzegh, and D. B. Parsons, "Size distribution of precipitation particles in frontal clouds," *J. Atmos Sci.*, vol. 36, pp. 156–162, 1979.

[30] S. M. Sekelsky, W. L. Ecklund, J. M. Firda, K. S. Gage, and R. E. McIntosh, "Particle size estimation in ice-phase clouds using multifrequency radar reflectivity measurements at 95, 33, and 2.8 GHz," *J. Appl. Meteorol.*, vol. 38, pp. 5–28, 1999.

[31] R. Bennartz and G. W. Petty, "The sensitivity of microwave remote sensing observations of precipitation to ice particle size distributions," *J. Appl. Meteorol.*, vol. 40, pp. 345–364, 2001.

[32] F. T. Ulaby, R. K. Moore, and A. K. Fung, *Microwave Remote Sensing Active and Passive*. Reading, MA: Addison-Wesley, 1981, vol. 1, Microwave Remote Sensing Fundamentals and Radiometry.

[33] J. Weinman, "The effect of Cirrus clouds on 118-GHz brightness temperatures," *J. Geophys. Res.*, vol. 93, no. D9, pp. 11 059–11 062, 1988.

[34] L. Roberti and C. Kummerow, "Monte Carlo calculations of polarized microwave radiation emerging from cloud structures," *J. Geophys. Res.*, vol. 104, pp. 2093–2104, 1999.

[35] C. Kummerow, "Beamfilling errors in passive microwave rainfall retrievals," *J. Appl. Meteorol.*, vol. 37, pp. 356–370, 1998.

[36] P. Bauer, L. Schanz, and L. Roberti, "Correction of the three-dimensional effects for passive microwave remote sensing of convective clouds," *J. Appl. Meteorol.*, vol. 37, pp. 1619–1632, 1998.

[37] Q. Liu, C. Simmer, and E. Ruprecht, "Three-dimensional radiative transfer effects of clouds in the microwave spectral range," *J. Geophys. Res.*, vol. 101, pp. 4289–4298, 1996.

[38] H. Czekala, P. Bauer, D. Jones, F. Marzano, A. Tassa, L. Roberti, S. English, J. P. V. Poiares Baptista, A. Mugnai, and C. Simmer, "Clouds and precipitation. COST Action 712: Radiative transfer models for microwave radiometry, Final Report of Project 1," Directorate-General for Research, Eur. Commiss., Brussels, Belgium, EUR 19543 EN, C. Maetzler, Ed., 2000.

[39] P. Bauer, A. Kahin, A. Pokrovsy, R. Meneghini, C. Kummerow, F. S. Marzano, and J. P. V. Poiares Baptista, "Combined cloud-microwave radiative transfer modeling of stratiform rainfall," *J. Atmos. Sci.*, vol. 57, pp. 1082–1104, 2000.

[40] F. S. Marzano and P. Bauer, "Sensitivity analysis of airborne microwave retrieval of stratiform precipitation to the melting layer parameterization," *IEEE Trans. Geosci. Remote Sens.*, vol. 39, no. 1, pp. 75–91, Jan. 2001.

[41] P. Bauer, "Including a melting layer into microwave radiative transfer simulation for cloud," *Atmos. Res.*, vol. 57, no. 1, pp. 9–30, 2001.

[42] W. S. Olson, P. Bauer, N. F. Viltard, D. E. Johnson, W. K. Tao, R. Meneghini, and L. Liao, "A melting layer model for passive/active microwave remote sensing applications. Part II: Simulation of TRMM observations," *J. Appl. Meteorol*, vol. 40, pp. 1164–1179, 2001.

[43] C. J. Walden, G. Kuznetsov, and A. R. Holt, "Scattering properties of hydrometeors: Modeling requirements," ESA, Noordwijk, The Netherlands, Interim Report on Contract ENV4-CT97-0421, 1999.

[44] R. A. Houze, *Cloud Dynamics*, ser. International Geophysics Series. San Diego, CA: Academic , 1993, vol. 53.

[45] H. R. Pruppacher and J. D. Klett, *Microphysics of Clouds and Precipitation*. Amsterdam, The Netherlands: Reidel, 1978.

[46] J. L. Haferman, "Microwave scattering by precipitation," in *Light Scattering by Non-Spherical Particles: Theory, Measurements and Applications*, M. I. Mishchenko, J. W. Hovenier, and L. D. Travis, Eds. New York: Academic, 1999, pp. 481–502.

[47] H. Czekala, S. Crewell, C. Simmer, A. Thiele, A. Hornbostel, and A. Schroth, "Interpretation of polarization features in ground-based microwave observations as caused by horizontally aligned oblate raindrops," *J. Appl. Meteorol.*, vol. 40, pp. 1918–1932, 2001.

[48] C. D. Kummerow and J. A. Weinman, "Radiative properties of deformed hydrometeors for commonly used passive microwave frequencies," *IEEE Trans. Geosci. Remote Sens.*, vol. 26, pp. 629–638, Sep. 1988.

Alessandra Tassa received the laurea degree (cum laude) in telecommunications engineering and the Ph.D. degree in remote sensing from the University of Rome "La Sapienza," Rome, Italy, in 1998 and 2005, respectively.

Since 1999, she has been with the Institute of Atmospheric Sciences and Climate, Italian National Council for Research (CNR), Rome, working on precipitation estimation from TRMM data and simulation of microwave radiances over precipitating clouds. She is presently involved in the study for the definition of the optimal characteristics of the microwave radiometer to be mounted on the European satellite member of the planned Global Precipitation Measurement Mission.

Sabatino Di Michele received the laurea degree in electronic engineering and the Ph.D. degree in information and electrical engineering from the University of L'Aquila, L'Aquila, Italy, in 1997 and 2004, respectively.

Since the beginning of 1998, he has been collaborating with the Department of Electrical Engineering, University of L'Aquila, working on SSM/I applications and ground-based radiometry. In November 1998, he joined the Institute of Atmospheric Physics, CNR, Rome, Italy, to work on rainfall retrieval techniques for the Tropical Rainfall Measuring Mission (TRMM) microwave instruments. He is currently with the European Centre for Medium-range Weather Forecast (ECMWF), Reading, U.K., working on issues related to rainfall assimilation. He has been participating in various international projects (e.g., EuroTRMM, Eurainsat) concerning precipitation estimation from spaceborne microwave sensors. He is also involved in the research activity of the planned Global Precipitation Measurement Mission. His studies are mainly focused on radiative transfer modeling and on the development of new inversion procedures.

Alberto Mugnai, photograph and biography not available at the time of publication.

Frank Silvio Marzano (S'89–M'99–SM'03) received the laurea degree (cum laude) in electrical engineering and the Ph.D. degree in applied electromagnetics, in 1988 and 1993, respectively, both from the University of Rome "La Sapienza," Rome, Italy.

He joined the Department of Electronic Engineering, University or Rome "La Sapienza," in 2005, where he teaches courses on antennas, propagation, and remote sensing. In 1993, he collaborated with the Institute of Atmospheric Physics (CNR), Rome. From 1994 until 1996, he was with the Italian Space Agency, Rome, as a Post-Doctorate Researcher. After being a Lecturer at the University of Perugia, Perugia, Italy, in 1997, he joined the Department of Electrical Engineering, University of L'Aquila, coordinating the Satellite and Radar Remote Sensing Laboratory. His current research interests are passive and active remote sensing of the atmosphere from ground-based, airborne, and spaceborne platforms, with a particular focus on precipitation using microwave and infrared data, development of inversion methods, radiative transfer modeling of scattering media, and radar meteorology issues. He is also involved in radiopropagation topics in relation to incoherent wave modeling, scintillation prediction, and rain fading analysis along satellite microwave links. He has published more than 45 papers in refereed international journals and books and more than 170 extended abstract in international and national congress proceedings.

Dr. Marzano received the Young Scientist Award of the XXIV General Assembly of the International Union of Radio Science in 1993. In 1998, he was the recipient of the Alan Berman Publication Award from the Naval Research Laboratory, Washington, DC. Since 2001, he is the Italian National Delegate for the European COST actions number 720 on meteorological remote sensing and number 280 on satellite communications. He is an Associate Editor for IEEE GEOSCIENCE AND REMOTE SENSING LETTERS. In 2004, he was Co-Guest Editor of the special issue on MicroRad04 for IEEE TRANSACTIONS ON GEOSCIENCE AND REMOTE SENSING.

Peter Bauer, photograph and biography not available at the time of publication.

José Pedro V. Poiares Baptista, photograph and biography not available at the time of publication.